6th International Conference on Multiphase Flow,
ICMF 2007, Leipzig, Germany, July 9 – 13, 2007

A stochastic particle-particle collision model for dense gas-particle flows implemented in the Lagrangian solver of ANSYS CFX and its validation

Björn Hussmann*, Michael Pfitzner*, Thomas Esch‡ and Thomas Frank‡

*University of the Federal Armed Forces Munich, Faculty of Aerospace Engineering, Thermodynamics Institute

Werner-Heisenberg-Weg, 85577 Neubiberg, Germany

‡ANSYS Germany GmbH

Staudenfeldweg 12, 83624 Otterfing, Germany

michael.pfitzner@unibw.de, thomas.frank@ansys.com

Keywords: particle collisions, dense gas-particle flows, stochastic model

Abstract

In classical Euler-Lagrange modelling, collisions between particles are not possible since the presence of other particles is not accounted for. The stochastic particle-particle collision model by Oesterlé & Petitjean, extended by Sommerfeld, takes inter-particle collisions into consideration while the trajectories are still calculated sequentially. For the first time, this particle-particle collision model is implemented into and validated within a commercial CFD-code, viz. ANSYS CFX.
The main advantage of the model is the possibility of sequential trajectory calculation by creating virtual collision partners sampled from local statistical values. This offers a high potential of parallelisation and thus facilitates – in conjunction with the highly parallelised CFX-solver for the gas-phase – its use in industrial applications. The model extension by Sommerfeld additionally takes into account a possible correlation between the velocity fluctuations of neighbouring particles.
The implementation into ANSYS CFX was validated based on three published experiments. These comprise a convergent channel provoking inter-particle collisions, a highly loaded vertical pipe flow and a strongly swirling pipe flow. The implemented model yields satisfactory results with only minor additional computational effort. It represents a major advance in the simulation of dense gas-particle flows in commercial CFD-solvers and will be available in the forthcoming official releases of ANSYS CFX.

Introduction

Highly loaded gas-particle flows are commonly simulated by the two-fluid model with interactions between particles modelled based on the Kinetic Theory of Dense Gases. In classical Euler-Lagrange modelling the equations of motion of individual particles are solved where collisions between particles are not possible, since the presence of other particles is not taken into account.

The stochastic particle-particle collision model by Oesterlé & Petitjean (1993) extended by Sommerfeld (2001) takes inter-particle collisions into consideration while the trajectories are still calculated sequentially. For the first time this particle-particle collision model is implemented into and validated within a commercial CFD-code, viz. ANSYS CFX.

Standard Lagrange modelling is constrained to dilute two-phase flows since particles are independent of their neighbours. Activating this collision model facilitates the application of the Lagrange model to dense gas-solid flows with a high mass-loading while the particle volume fraction is still low. Hence dense multiphase flows in which contact forces between particles preponderate over aerodynamic forces exerted by the fluid, such as in fluidised beds or hoppers, are excluded. This is because the model is limited to binary collisions which dominate, if the average distance between two particles is much greater than their diameters.

Both the Euler-Euler multiphase model and the "classical" Euler-Lagrange model can approximate dense gas-solid flows only roughly. The newly implemented model expands the Euler-Lagrange model by a stochastic inter-particle collision model allowing for so-called *four-way coupling*. Hereby the mutual influence of gas and particles is accounted for as well as the mutual interaction of (spherical) particles by means of binary collisions.

The basic idea of the model is to track the particles sequentially and still to use information regarding other particles allowing for calculation of collisions. The sequential approach requires a supply of this information before the trajectories are calculated. For this purpose, the local mean and the standard deviation of certain values are gathered in each computational control volume after completion of the calculation of all particle trajectories. These include for example particle concentration and velocity as well as the fluctuating part of the velocity components. In the subsequent iteration these local stochastic data serve as a basis for the generation of a virtual collision partner, whose properties reflect the local average values, where applicable supplemented by a fluctuating part. This fictitious particle is generated anew in each Lagrangian step.

Furthermore, the probability of a collision between the current real particle and the virtual one is calculated from these data. A random process determines whether or not a collision occurs. If so, the collision amongst the two collision partners is calculated in a deterministic way providing new velocity components for the current real particle and discarding the fictitious one which is no longer of any use. If a collision does not take place the velocity of the real particle remains at the value calculated by the standard solver.

A simultaneous tracking of all particles would necessitate an examination of possible collisions among all particle pairs. This enormous complexity is avoided by application of the stochastic collision model. Nonetheless this is an iterative procedure, so the trajectory calculation has to be repeated several times with a changing gas flow field. The sequential approach followed here offers a high potential of parallelisation and thus facilitates – in conjunction with the highly parallelised CFX-solver for the gas-phase – its use in industrial applications.

The main focus of this work is the validation of the collision model implementation into ANSYS CFX based on three experiments from the literature to verify the greatly improved performance of simulations with the collision model compared to standard calculations without the model. Therefore experiments with dense gas-particle flows were selected. These included a convergent vertical channel provoking collisions (Fohanno & Oesterlé (2000)), a vertical two-phase pipe flow (Tsuji, Morikawa & Shiomi (1984)), and a strongly swirling pipe flow (Zhou *et al.* (2000)), each with different characteristics and challenges for the model.

While the implementation of the collision model can already account for particle rotation, the particle-wall collision treatment in the code ANSYS CFX cannot. Thus all results shown here were calculated without considering particle rotation. This ought to be kept in mind regarding the comparisons presented in this article.

The outline of the paper is as follows: Firstly, the algorithm of the collision model is presented in some detail to provide an understanding of the mode of operation. Secondly, the three validation cases are presented including a short description of the experimental configurations. The measured data are then compared to simulation results with the activated inter-particle collision model and in part also without the model to assess its effect.

Nomenclature

d_P	particle diameter (m)
f_c	collision frequency (s^{-1})
g	gravitational constant (ms^{-2})
$\vec{J}$	transferred momentum ($kgms^{-1}$)
m	mass loading
$\dot{m}_P$	particle mass flow rate (kgs^{-1})
n_P	particle number density (m^{-3})
P_c	collision probability
R	correlation function
Re	Reynolds number
S	swirl number
St_t	turbulent Stokes number
Δt	Lagrangian time step (s)
u_c	centre line velocity (ms^{-1})
v_j	instanteneous velocity (ms^{-1})
$\overline{v_j}$	mean velocity (ms^{-1})
v_j'	fluctuating velocity (ms^{-1})

Greek letters

ξ	random number (Gaussian)
σ_P	local mean fluctuating velocity (ms^{-1})
ψ	random number (uniformly distributed)

Subscipts

i	coordinates x, y, z or particle 1, 2

Collision model implementation

In each time step during a trajectory calculation the Lagrangian solver invokes the collision subroutine and provides the demanded variables. The subroutine decides whether or not a collision takes place. If so, the new particle velocity components are transferred back to the standard Lagrangian solver that incorporates the effect of the aerodynamical and body forces acting on the particle.

The variables to be passed to the collision subroutine consist of local mean values of translational velocity components and their mean fluctuating parts (standard deviation) from the previous Lagrange iteration. As a consequence, the first iteration of such a simulation has to be executed without incorporating particle collisions to supply the required averaged data.

Moreover, the local mean particle diameter and its standard deviation as well as the local particle number density have to be supplied. The diameter, location, and the instantaneous velocity of the current real particle and the Lagrangian time step have to be passed to the subroutine.

For the calculation of the instantaneous velocity of the virtual collision partner, a partial correlation of the turbulent fluctuation velocities between the real and the fictitious particle is taken into account, as proposed by Sommerfeld (2001). The correlation is a function of the turbulent Stokes number St_t which is the ratio of the aerodynamic relaxation time and a characteristic eddy lifetime, the latter provided by the turbulence model. Small particles being able to follow the gas flow easily have Stokes numbers below unity, the Stokes numbers of large inertial particles exceed unity.

Sommerfeld's correlation function,

$$R\left(\mathrm{St}_t\right) = \exp\left(-0.55\,\mathrm{St}_t^{0.4}\right) \,, \tag{1}$$

which was adapted to LES-data of a homogeneous isotropic turbulence field by Lavieville *et al.* (1995) is used to determine the fluctuating velocity of the fictitious collision partner

$$v_{2,i}' = R\left(\mathrm{St}_t\right)\, v_{1,i}' + \sigma_{P,i}\sqrt{1 - R\left(\mathrm{St}_t\right)^2}\,\xi \,, \tag{2}$$

where the index 1 stands for the real particle and index 2 for the virtual particle, index i represents the three coordinate directions and the prime indicates a fluctuating part of the velocity. $\sigma_{P,i}$ is the i-th component of the mean fluctuation velocity in the control volume. ξ is a Gaussian random number with zero mean and standard deviation of unity. It represents the uncorrelated part of the fluctuation velocity of the fictitious particle. Its instantaneous velocity is simply the sum of the fluctuating part described above and the local mean value.

The collision frequency is then determined in analogy to the Kinetic Theory of Gases, Oesterlé & Petitjean (1993), by means of the equation

$$f_c = \frac{\pi}{4}\,(d_{P1} + d_{P2})^2\,|\vec{v_1} - \vec{v_2}|\,n_P\,, \tag{3}$$

where $\vec{v_1}$ and $\vec{v_2}$ represent the instantaneous velocities of real particle 1 and its collision partner 2. The diameter of the latter is sampled from a Gaussian distribution around the local average value.

The collision probability being a simple function of collision frequency and Lagrangian time step can now be calculated

$$P_c = 1 - \exp\left(-f_c\,\Delta t\right)\,. \tag{4}$$

The time step can be altered in the collision subroutine to ensure accuracy and stability of the calculation by limiting it to $\Delta t \leq 0.05/f_c$. This allows for at most one binary collision per time step, as derived by Sommerfeld (1995). Due to implementation constraints, the new time step first applies in the next Lagrangian step of the real particle, but the implied error is only of significance when the spatial gradient in collision frequency is high. This can be diminished by more Lagrangian steps per control volume.

A uniformly distributed random number $\psi \in [0,1]$ is then generated and compared to the collision probability P_c. If $P_c > \psi$ the inter-particle collision is calculated deterministically. If this is not the case, no collision occurs and the velocity components of the real particle remain unchanged.

In case of a collision, the location of the virtual particle has to be determined in a stochastic way. This is carried out in a local coordinate system to generate the collision partner relative to the location of the real particle. The position is sampled randomly from a uniform distribution on the collision cylinder cross section and a distance of the centre point according to the sum of the two particle radii. Subsequently, the position of the fictitious particle is transformed back to the global system. A more detailed description is given in Frank (2002).

At this stage, information on location, size and velocity of the virtual collision partner is known. The next step is to determine the change in the velocity components caused by the collision. For this purpose, it is again suitable to use a local coordinate system, different to the one mentioned above and fixed to the real particle. To identify the post-collision velocities, the momentum $\vec{J}$ transferred between the particles has to be determined. Here a distinction has to be made between a sliding and a non-sliding collision, if particle rotation is accounted for which affects the tangential components of $\vec{J}$. During a non-sliding collision the relative movement at the point of contact ceases whereas during a sliding collision, relative motion of the contact surfaces is maintained under the influence of sliding friction.

Besides the coefficient of restitution e considering the losses normal to the plane of contact, the coefficients of sliding and static friction have to be supplied for the particle material, if particle rotation is taken into account. Hence, in the case of rotating particles, a decision between the two collision modes is made based on the coefficient of static friction. The respective components of the transferred momentum are determined and the post-collision velocity components are calculated in the local coordinate system. Finally these values are transformed back to the global coordinate system and passed to the Lagrangian solver.

As soon as this is completed, the Lagrangian solver proceeds to the next time step, calculates the new velocities determined by the governing forces without collision and again calls the collision subroutine until the current trajectory is finished. Afterwards it starts the next particle trajectory till the last particle has been tracked through the computational domain.

Eventually the solver calculates and updates all necessary average and standard deviation values required by the collision model in each control volume. For a comprehensive derivation refer to Frank (2002).

Below all necessary steps of the algorithm are summarised. The scheme comprises the following items, cf. figure 1:

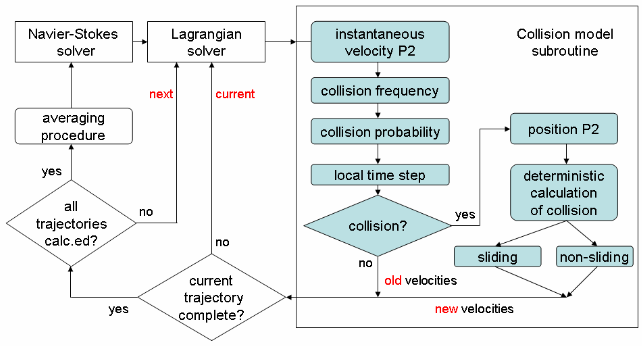

Figure 1: Schematic of the collision model algorithm.

- Call to the collision subroutine by the Lagrangian solver supplying the necessary variables.
- Calculation of the instantaneous velocity of the virtual collision partner.
- Determination of the collision probability and decision whether or not a collision occurs.
  - If a collision takes place
    - the position of the virtual collision partner is determined and
    - the binary collision is calculated deterministically;
  - if there is no collision the velocities remain unchanged.
- The fictitious particle is discarded.
- The trajectory calculation of the current real particle is continued until it is completed.

- For all trajectories the averaging procedure is carried out to obtain local statistical moments in each control volume.

Results and Discussion

After implementation and functional verification, the particle-particle collision model described above was validated based on three published experiments. Results of the calculations are compared to the measurements in the following subsections and potential sources of error in modelling and experiment are highlighted.

Case I

The first validation experiment was conducted by Fohanno & Oesterlé (2000). It was selected since its second author is one of the developers of the original collision model in Oesterlé & Petitjean (1993) and this experiment was established specifically for the purpose of model validation, thus all requirements were known. In this experiment, rather

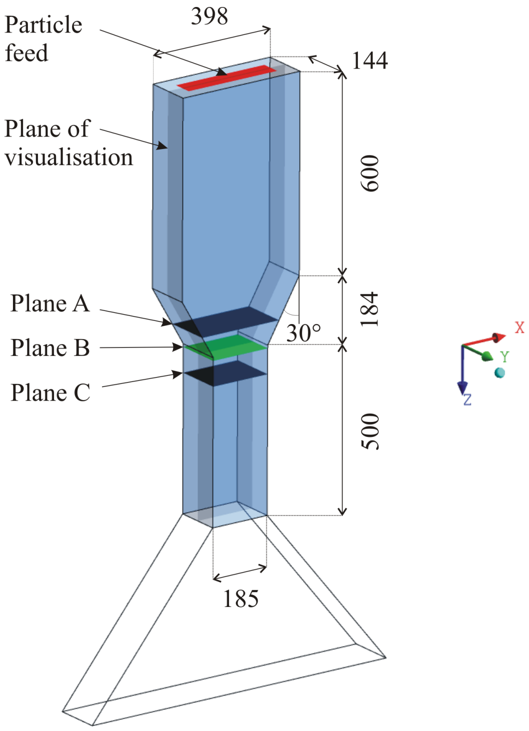

Figure 2: Simulated geometry in case I, dimensions in mm.

coarse and hence inertial particles, 3 mm in diameter, fall freely in a convergent channel due to gravitation. The channel has a rectangular cross-section and two of the walls, inclined by 30° to the vertical, form a convergent middle section. The geometry and the dimensions are shown in figure 2. The particles are fed into the channel through a vibrating perforated plate at the top in the marked area, $300 \times 60\ mm^2$ in size. Their initial velocity is about 0.2 m/s and in the upper part of the channel, they fall freely in air at atmospheric pressure. The particles are made of glass, having a density of 2500 kg/m^3, and are spherical in shape. A certain fraction of the particles hit the inclined walls at an approximate speed of 3.5 m/s, so their trajectories are deflected by particle-wall collisions. The channel itself is made of smooth glass, thus a deterministic wall-collision behaviour was expected. Nevertheless, due to attrition, this might not be the case after a longer period of operation as a certain wall roughness will emerge. The trajectories of the rebounding particles intersect with those of the particles falling vertically leading to regions of higher particle concentration and thus increased collision frequency further downstream. Here, with the walls being again parallel, the flow remains dominated by interparticle collisions. At the bottom, the particles exit the channel into the environment (the trapezoidal part shown in figure 2).

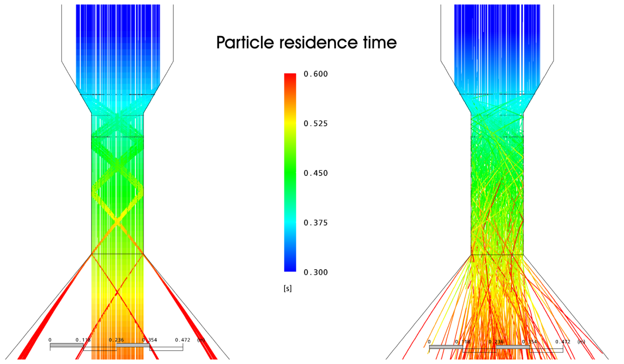

Figure 3: Particle trajectories without (left) and with (right) inter-particle collisions.

Figure 3 shows the particle trajectories for the case without (left) and with (right) inter-particle collisions. They are coloured by the particle residence time visualising the different origin of the particles downstream of the convergent part. Without taking into account inter-particle collisions, there is no information about surrounding particles during the calculation of their paths. Thus they cross unhindered, describing a zig-zag pattern caused by wall collisions or falling vertically, as can be seen in the left part of figure 3. By contrast the right hand side shows the trajectories when the stochastic collision model is activated. Due to the elevated collision frequency in regions of high particle concentration, a large number of collisions take place leading to a more or less homogeneous downward flow of particles depending on the particle mass flow.

For the measurements an optical technique called particle streak velocimetry was used. This is a two-dimensional method which was applied in the central plane of visualisation, as shown in figure 2. This method is capable of determining particle concentration and velocities. The experimental values were gathered at three levels in the channel, marked plane A to C in the same figure. In plane A a large number of particle-wall collisions occurs, being the first wall-contact for the particles. Plane B contains the crossing point of the trajectories of the rebounding particles in the channel centre, cf. also figure 3. In plane C the particles rebounding from the left wall reach the opposite wall for the first time and vice versa. Because of symmetry, measurements were only taken in the left half of the planes A to C.

During the experiments two particle mass flow rates $\dot{m}_P$, 0.13 and 0.38 kg/s, were selected. The lower rate leads to an appreciable number of inter-particle collisions while many particles may still fall unhindered, resulting in a particle volume fraction of $6.5 \cdot 10^{-4}$ downstream of the convergent part. Employing the higher flow rate yielding a volume fraction of $1.9 \cdot 10^{-3}$, almost every particle undergoes at least one collision. Nonetheless the mass loading is in a range where binary collisions prevail, as required by the model.

For the calculations a stationary state was assumed, and the air was modelled as incompressible isothermal fluid at room temperature. Turbulence was taken into account by means of the k-ε-model, but with the low air velocity, the turbulence intensity is slight and its influence on the particles even weaker since rather large particles were used to suppress this effect. The two-way coupling between gas and particles was established by taking buoyancy and drag forces into account, the latter inducing a downward air flow through the open channel. The particle motion was further influenced by the gravitational force and a turbulent dispersion term. The wall restitution coefficient was measured by Fohanno & Oesterlé to be $e = 0.96$, parallel to the wall no losses were taken into account. Due to a lack of data, the restitution coefficient for inter-particle collisions was also taken to be $e_{\mathrm{PP}} = 0.96$ since it represents the same material pair. The computational grid consists of about 620000 control volumes, approximately half a million trajectories were calculated during each Lagrange-iteration. A grid refinement study was conducted and no visible change between the results was detectable for the two finest grids, whereof the finer is used for presenting the results.

The validation is carried out with the new collision model in ANSYS CFX and the experimental data of Fohanno & Oesterlé. Further comparison is achieved with simulation data of Fohanno *et al.* themselves and calculations of Pachler (2004) who used the university CFD-code Mistral-Partflow3D which is capable of taking into account particle rotation. Consequently differences due to implementation or the effect of particle rotation can be identified.

Fohanno *et al.* estimated the experimental error as follows: For the measurement statistics, 28 photographs were evaluated for the smaller mass flow rate and 20 images for the higher mass flow leading to 25 to 130 trajectories per evaluation cell, i.e. per data point. The error in the particle mean velocities amounts to $\pm 13\%$ for the small and $\pm 10\%$ for the larger mass flow; the error in the velocity standard deviations totals $\pm 20\%$ for the lower and $\pm 15\%$ for the higher mass flow rate, respectively, according to the 95% confidence interval.

Figure 4(a) shows dimensionless concentration profiles in the left half of the channel in the plane of visualisation. The subfigures represent results in the three planes of measurement A to C, cf. figure 2. Each subfigure contains experimental data and calculated values for both particle mass flow rates.

The concentration can also be recognised on the basis of the trajectories in figure 3. In the upper two subfigures of figure 4(a) one can see that, qualitatively, the profiles are reproduced correctly, but the calculation results show in part considerable deviation. This holds also for the third subfigure in which the trend in the profile for the larger mass flow

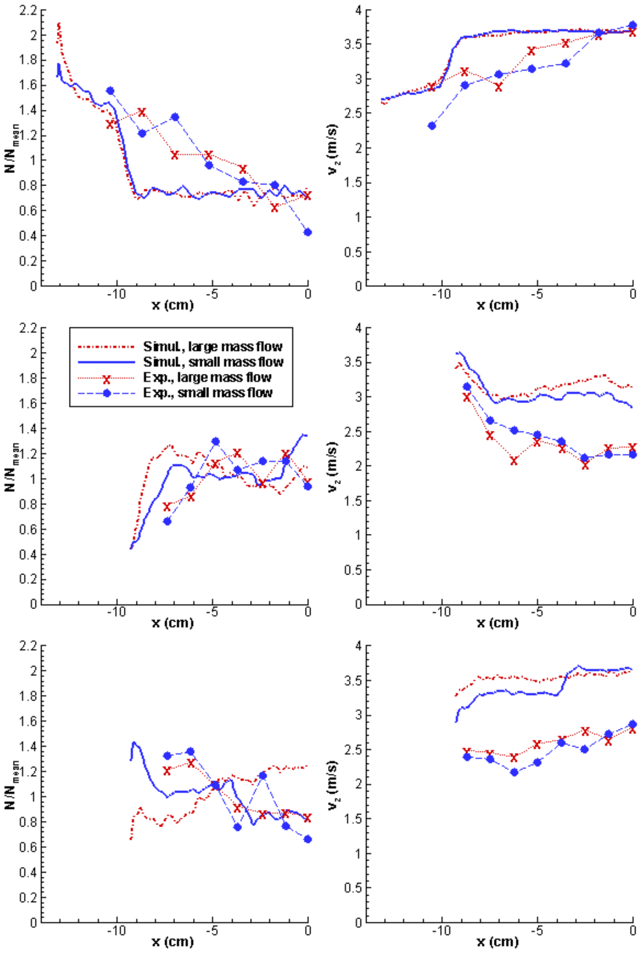

(a) Particle concentration (b) Axial velocity

Figure 4: Dimensionless concentration and axial velocity profile of particles as function of particle mass flow rate and axial position (planes A, B, and C from top to bottom).

is even contrary to the experiment.

In plane A a higher particle concentration arises close to the wall, as particles are reflected after their first wall contact and they slow down. In plane B, or curtly below, the trajectories cross midway between the walls and lead to a higher concentration in the channel centre. The particles coming from the opposite wall produce a higher concentration near the wall in plane C. For the larger mass flow this is not the case in the simulation since herein the crossing point of the trajectories lies between planes B and C and thus below the real point in the experiment. Close inspection of figure 3 shows that even a slight shift of the concentration maximum upwards would yield a better agreement. The reason for this deviation could be due to the simplified particle-wall collision treatment, as the wall roughness and friction were not taken into account. This influences the trajectories especially in the upper part of the channel.

Figure 4(b) displays the axial mean velocity profile of the particles, i.e. in the vertical direction, in the left half of the channel. In all three subfigures the trend of the experimental values is reflected properly but the values are considerably overpredicted. A possible reason for this phenomenon could

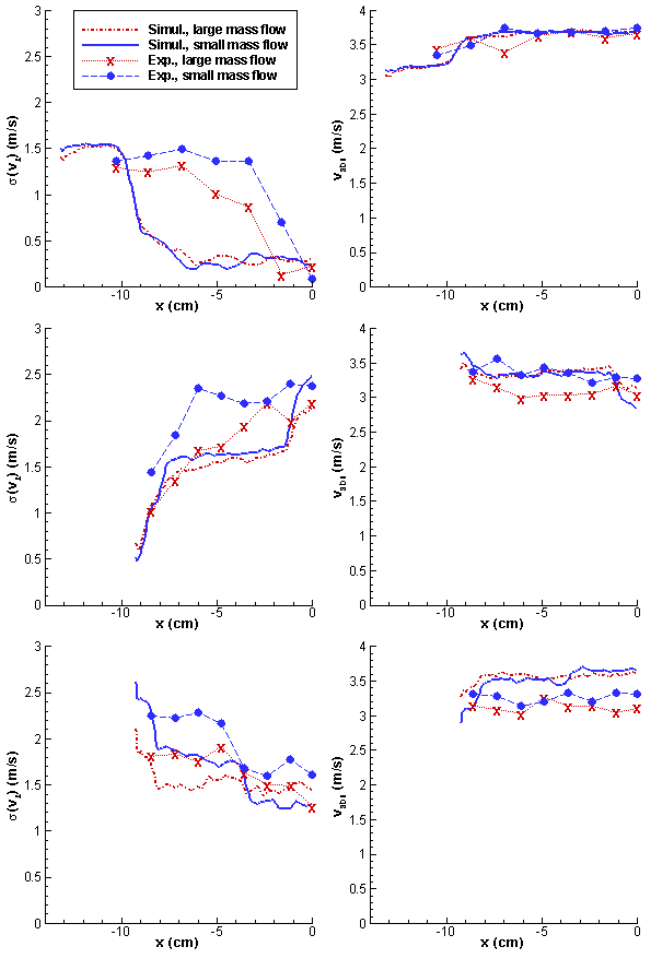

(a) Std. deviation, transverse vel. (b) Abs. value of velocity

Figure 5: Particle velocity profiles as function of particle mass flow rate and axial position (plane A to C from top to bottom).

be that the boundary condition for air at the channel top was set to entrainment in the calculation while in reality it was covered – at least in part – by the perforated plate limiting the possible air flow. Thus, in the real arrangement, a slow air circulation within the channel from bottom to top might have established contrary to the calculated pure downward flow in the simulation. Hence the drag force on the particles might be higher on the average impeding downward flow.

Fohanno & Oesterlé (2000) also overpredict the axial velocity in their own simulation. They attribute the effect to a potentially inappropriate value of the coefficient of static friction for the particle-wall collision. This value distinguishes between sliding and non-sliding collision and thus influences particle rotation which is not considered in our implementation.

The standard deviation of the transverse velocity, i.e. in horizontal direction x, as a measure of velocity fluctuations is shown in figure 5(a). For this entity the calculation also yields qualitatively correct profiles, except in the uppermost plane A. Though there is a decrease towards the channel centre, the calculated velocity fluctuations are generally much lower than the experimental values. The standard deviation in plane A close to the wall is 1.5 m/s because of particle-wall collisions and approximately zero in the channel centre, where all particles fall vertically. In plane B particles rebounding from the walls cross leading to transverse relative velocities of about 4 m/s and a standard deviation of 2.5 m/s. For plane C a homogenisation can be observed.

This deviation between experimental and calculated values in plane A can be explained only to a minor degree by particle-wall collisions. Potentially measurement errors prevail since it can be seen from figure 3 that except directly at the wall only vertically oriented trajectories occur. The experimental values imply existence of considerable transverse motion of particles at that position in the channel which cannot be explained in terms of geometry. Interestingly the calculations of Pachler (2004) show similar results as shown here, also far below the measured values for plane A. The only explication for such a high velocity fluctuation even before impacting on the wall for the first time would be inter-particle collisions already in the upper part of the channel. This could be due to considerable gas turbulence – which is improbable – or, more likely, due to vibrational motion of the perforated plate used as a particle feed. In their paper Fohanno & Oesterlé sketched a feeding device that is only vibrating vertically, but obviously a transverse fluctuation was imposed on the particles.

These authors underestimate the standard deviation in transverse direction in their own simulation as well. They explained the differences by a potentially erroneous specification of the coefficient of static friction for the wall whereby the boundary between sliding and non-sliding collision is shifted. Based on the above reasoning, this is not a sufficient rationale, at least for plane A.

In plane B the location of the maximum in the calculated velocity fluctuations is closer to the channel centre. This is again caused by a too low crossing point of the trajectories, as compared to the experiment. For the same reason the differences arise in plane C.

Furthermore it can be found that the concentration profile and the axial velocity are quite uncorrelated to the particle mass flow rate while the intensity of velocity fluctuations in transverse direction, especially at the bottom plane, is at a lower level at a higher mass flow. Augmentation of the particle mass flow rate involves a rise in the collision frequency leading to a damping of the fluctuations because of non-elastic material behaviour.

Figure 5(b) shows the absolute value of particle velocity in the plane of visualisation $V_{\text{abs}} = \sqrt{V_x^2 + V_z^2}$. While the accordance with the experimental values is very good in plane A and for the lower mass flow also in plane B, more pronounced deviations appear in plane C. The results of the simulation do not predict a reduction of the absolute velocity value whereas this can clearly be seen in the experimental values.

This might be due to three reasons. Firstly, all collisions are three-dimensional and hence also a motion normal to the plane of visualisation in y-direction is possible which is not accounted for in calculating the absolute value since the measurement technique is two-dimensional. An analysis of this point showed that the contribution of particle velocities in y-

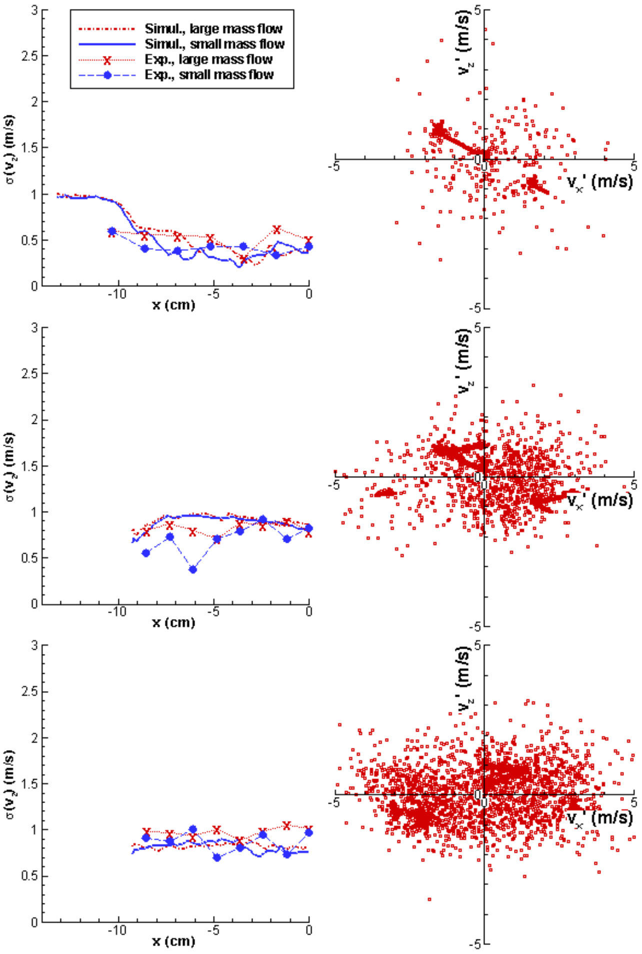

(a) Std. deviation, axial vel. (b) Velocity fluctuations

Figure 6: Profile of axial particle velocity fluctuations (a) as function of particle mass flow rate and axial position and scatter plot of axial and transverse particle velocity fluctuations (b) at the lower mass flow rate as a function of axial position (plane A to C from top to bottom).

direction is negligible (less than 0.05 m/s). A second reason could be losses by virtue of non-elastic collisions between the particles and with the walls. However with a measured coefficient of restitution of $e = 0.96$ virtually elastic rebounding is achieved. So the main cause of velocity decrease in the experiment would be the conversion of translational into rotational kinetic energy of the particles by means of collisions involving friction. The results of Pachler point towards this supposition as he took particle rotation into account for in his calculations and his results are closer to the experimental data.

The decline seems to depend on the number of collisions which supports the third reason as well. With a higher mass flow rate of particles and thus a larger number of energy-transforming collisions, the losses are already visible in the experimental values in plane B and maintain that level in the more homogenised flow. In contrast, at the smaller flow rate, this lower level is not reached until plane C when more collisions will have occured.

In figure 6(a) profiles of the standard deviation of velocity fluctuations in axial, i.e. vertical, direction are depicted. For this quantity the results of the calculations coincide with the experimental values within the accuracy of measurement. Concerning this feature our calculations are closer to the experimenal data than the results of Pachler. The values amount to approximately 1 m/s after initiation of the collision process. In plane C a slight increase in the standard deviation can be observed with the higher mass flow rate. This indicates a reduction of the initial anisotropy of the velocity fluctuations as a result of the collisions.

The last quantity to be analysed is the illustration of the fluctuating part of the particle velocities in a scatter plot as presented for the experimental values in Fohanno & Oesterlé (2000). For all three measurement planes A, B and C, the axial velocity fluctuation of each particle was plotted as a function of its transverse fluctuation. For the respective plane all particles from the left wall to the channel centre, i.e. only the left half of the channel, were considered. The instanteneous velocity of the particle v_i comprises a mean part and a fluctuating part

$$v_i = \overline{v_i} + v_i', \tag{5}$$

where $\overline{v_i}$ is the i-th component of the average velocity in the considered control volume, and v_i' is the fluctuating part in direction i. The latter is shown in figure 6(b). Here only the simulation results for the lower particle mass flow rate are shown which display a larger scatter than the experimental values shown in Fohanno & Oesterlé (2000) since the number of data points shown here is more than one order of magnitude higher (≈ 5000 points, randomly selected).

In plane A two types of particle trajectories dominate. The first type accords to particles falling vertically, the second to particles rebounding from the left wall in an oblique direction. For the particles falling freely the x-component of their instanteneous velocity v_x is zero, hence compared to the average value in the control volume, their transverse deviation v_x' is negative. The axial difference to the mean is positive $v_z' > 0$ since they fall more quickly than the particles with oblique trajectories. Thus these points are to be found in the second quadrant in the scatter plot. Particles rebounding from the left wall have a positive instantaneous velocity in the transverse direction $v_x > \overline{v_x} > 0$. Hence $v_x' > 0$ and as they fall more slowly, $v_z' < 0$, so these points are located in the fourth quadrant. The alignment results in a characteristic oblique direction. A number of particles do not belong to any of these groups and are distributed dispersely. These had already undergone collisions with other particles.

Comparison between calculated and experimental results shows that the locations of accumulation and the characteristic direction are reproduced accurately. The sporadical dispersed points exhibit a larger scatter than in the experiment, but one has to take into account the larger number of events shown in the calculation. With a higher particle mass flow rate the dispersion increases as a consequence of a higher collision frequency.

In plane B the situation has changed. Trajectories close to the wall produce two accumulation points as in plane A along a characteristic direction. Near the wall there are less particles in this plane as the majority is located in the channel centre rebounding from both left and right walls yielding a higher particle concentration. Symmetry leads to a vanishing mean velocity in the transverse direction $\overline{v_x} = 0$. For the particles falling vertically, therefore, $v'_x \approx 0$, $v'_z > 0$ and for particles reflected by the walls $v'_x \approx v_x$, $v'_z < 0$. Hence this yields three points of accumulation but in plane B a larger number of particles deviate from these points after having undergone one or more inter-particle collisions. This effect becomes even more apparent for the larger particle mass flow rate (not shown here). Also for plane B the calculated accumulation points coincide with the experimental values and display a larger scatter because of a higher number of selected trajectories. Furthermore it is obvious that the velocity fluctuations in the axial direction are lower than in the transverse direction, as has been shown in figures 5(a) and 6(a).

In plane C particles coming from the right wall reach the left wall for the first time. Although the three groups described for plane B still prevail, more and more glass pearls separate from these groups. Because of the high number of collisions a homogenisation of the fluctuating velocities can be observed, again more pronounced for the higher mass flow. Still the fluctuations have a larger amplitude in transverse than in vertical direction. The results of our calculations reproduce these effects very well, also quantitatively. It is found that in plane C, fewer particle trajectories differ from the rest in the transverse fluctuations, i.e. the velocity fluctuations are damped by the collisions.

To conclude the validation on the basis of case I, taking into account particle-particle interactions is crucial for this type of geometry. The calculations with the implemented collision model correctly reflect the behaviour to a good approximation. Velocity profiles, homogenisation of the flow and damping of velocity fluctuations as well as the influence of the particle mass flow are predicted qualitatively in agreement with the measurements. Nonetheless some deviation emerges as a consequence of several factors.

Firstly, particle-wall collisions have a decisive influence in the upper part of the channel since they dictate the first crossing point of the particle trajectories and thus their subsequent path. In the implementation into ANSYS CFX as conducted here, there is no possibility of taking into account a particle-wall collision including friction which would yield a rotating particle. But also in the calculations of Fohanno & Oesterlé (2000) and Pachler (2004) who did consider the rotation, differences compared to the experiment are found, even if a slight improvement is achieved compared to the calculations shown here. A potentially inadequate choice of the coefficient of static friction can only explain the deviations in part.

In abandoning particle rotation, no rotation-induced lift forces influencing the particle motion, such as the Magnus force, could be taken into account. The Saffman force was neglected as well since no pronounced shear layers were expected in this configuration. Pachler calculated the differences between the original model by Oesterlé & Petitjean (1993) and the extended model by Sommerfeld (2001), the latter considering correlation between velocity fluctuations of neighbouring particles and being current model implemented in ANSYS CFX. The extended model shows a slight improvement for this case, although the fraction of correlated movements is expected to be low as the glass particles are rather large and the turbulent Stokes number is about 7.

Case II

The second case used for validating the inter-particle collision model implemented in ANSYS CFX was published by Tsuji, Morikawa & Shiomi (1984). This article describes an upward vertical flow in a 30.5 mm inner diameter pipe of 5 m length. The air-particle two-phase flow developed slip between the phases induced by gravitation.

For the measurement of the velocity profiles of gas and particles, use was made of Laser Doppler Anemometry (LDA). The tracer particles for determining the gas velocity had a mean diameter of 0.6 μm differing by 2-3 orders of magnitude to the particles of the second phase. This optical measuring method requires the laser beam to penetrate the measuring volume, especially so if the system is operated in forward scattering mode as was done here. The application of this method was impeded here since mass loadings of up to $m = 5$ were examined.

The same group of authors published a similar study for a horizontal pipe flow, Tsuji & Morikawa (1982). For the validation of the collision model, the vertical arrangement was preferred since in the vertical flow the results are less biased by factors of secondary importance such as particle-wall collisions than in the horizontal case. In the latter, gravition induces frequent collisions with the lower wall that might lead to deposition.

Of note in the experimental set-up is the following. The initially homogenised horizontal flow is bent upwards in an elbow which is combined with a forward facing step, i.e. a reduction of the cross section to redisperse the particles. Nevertheless the correct functionality of this device was not validated by Tsuji *et al.*, so particle strands and other regions of high particle concentration cannot be excluded. Besides no concentration profiles were measured.

Examination of the velocities was only performed at the top of the vertical pipe at a height of 5.11 m. Tsuji *et al.* report that there were no differences between velocity profiles in the last section of the pipe so they assumed a fully developed flow at this position.

For the validation of the collision model three of the large number of results in Tsuji, Morikawa & Shiomi (1984) were selected, as summarised in table 1. Three different particle diameters were investigated, viz. 3 mm, 500 μm, and 240 μm, so the largest particles take up almost a tenth of the pipe diameter. The spherical particles in the experiment consisted of polystyrene with a density of 1020 kg/m^3, considerably lighter than the glass spheres in validation case I. For the same mass loading this yields a higher volume fraction of the particles as compared to glass and represents a disadvantage for the optical measurement technique. Table 1 comprises specification of gas and particle mass flows and the centreline velocity u_c used for scaling in the diagrams below.

For the numerical investigation a stationary pipe flow in a 10 m long vertical pipe was established. The twofold length

	Case IIa	Case IIb	Case IIc
d_P [μm]	2780	501	243
Re	31000	16000	30000
$\dot{m}_G$ [g/s]	13.5	6.98	13.09
$\dot{m}_P$ [g/s]	40.5	13.96	27.49
m	3.0	2.0	2.1
$v_{P,in}$ [m/s]	9.0	6.0	12.5
u_c [m/s]	19.5	9.0	17.4

Table 1: Parameters of validation experiments for case II, vertical pipe flow.

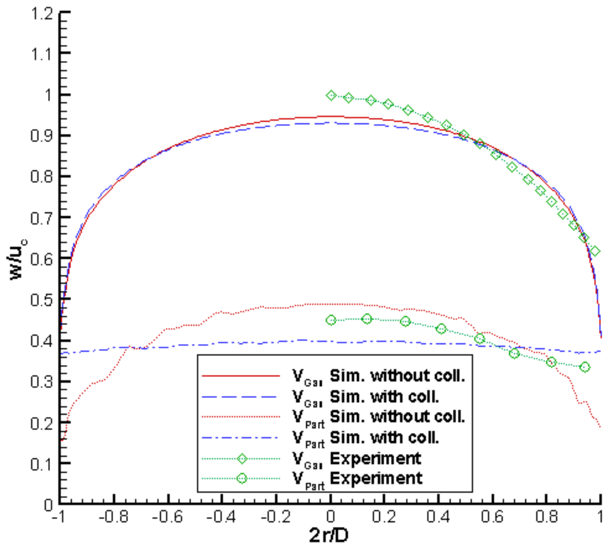

Figure 7: Comparison of calculated and experimental values for the axial velocities of gas and particles for case IIa. Mass loading m = 3.0, particle diameter d_P = 2.78 mm, Re $\approx$ 31000, centreline velocity u_c = 19.5 m/s.

of the pipe was selected to verify the fully developed flow after 5 m as stated by Tsuji *et al.* The computational grid was made up of over one million control volumes, fine enough to resolve the boundary layer. Below, results are shown for calculations with and without the activated collision model to examine the potential differences.

Similar to validation case I, air was treated as an isothermal gas at room temperature and pressure, the particle properties were set according to the values indicated in table 1. The physical models applied were the same as in case I except gas turbulence which was taken into account by a combined k-ε- and k-ω-model. Of note is the boundary condition at the lower pipe end where plug flow was assumed in the simulation. By contrast in the experiment, the elbow and step were located at this position leading to a disturbed flow regime. In each iteration 50000 particle trajectories were calculated.

Information on the coefficient of restitution for polystyrene particles of similar size on acrylic glass walls were taken from Frank (2002) and were originally published by Tsuji's group, Tsuji *et al.* (1987). In our simulation, due to a lack of experimental data, the value of e = 0.80 was used for particle-particle collisions as well. Particle rotation was not considered in the calculations for case II.

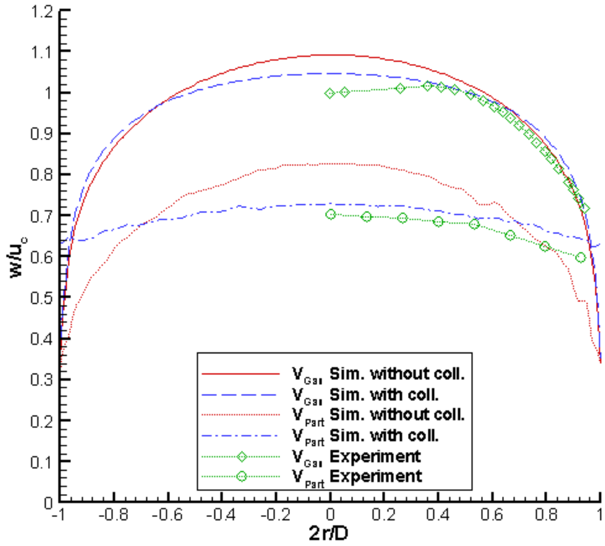

Figure 8: Comparison of calculated and experimental values for the axial velocities of gas and particles for case IIb. Mass loading m = 2.0, particle diameter d_P = 501 μm, Re $\approx$ 16000, centreline velocity u_c = 9.0 m/s.

Figure 7 displays the velocity profiles of the gas-phase and the particles at the top end of the vertical pipe for the simulation with and without the collision model in addition to the experimental values of Tsuji *et al.* for case IIa with the largest particles used (d_P = 2.78 mm). With an activated collision model, a homogenisation of the flow can be observed, the profile for the particles is much flatter than without taking collisions into account. The comparison with the experimental data shows that the calculated profile for the particles is slightly too flat with a deviation of about $\pm 10\%$. In the pipe centre, the simulation results without collisions are even closer to those measured but the flow near the wall is represented in a better way by including collisions; there is not such a steep decay as without the model.

The gas velocity does not differ markedly between both calculations. With the activated collision model, the gas phase is also decelerated slightly due to the lower particle velocity. Nevertheless the experimentally observed profile depicts higher gas velocities in the pipe centre and lower velocities near the wall than in the simulations. Only directly at the wall there is stronger curvature of the calculated profile, falling below the experimental values again.

The mass loading in case IIa is $m = 3.0$ and thus the highest in the calculations shown here. At such a high value, the optical measurement technique is already near its limits of application. Additional potential sources of error are addressed further below.

Velocity profiles of gas and particles for case IIb are summarised in figure 8. Here the average particle diameter is $d_P = 501$ μm. As can be seen from the figure, the particle velocity profile is represented very well by the calculation with activated collision model. The differences amount to only 3-6%. Without collisions the predicted particle velocity is completely incorrect, too high in the centre and too low near the wall. The collision model demonstrates its superior-

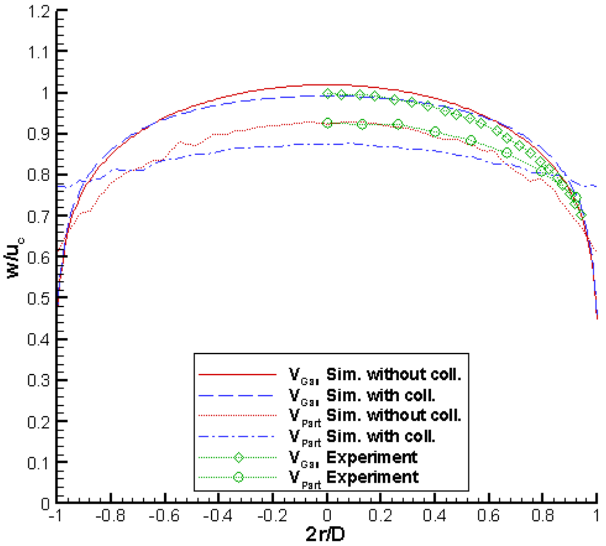

Figure 9: Comparison of calculated and experimental values for the axial velocities of gas and particles for case IIc. Mass loading m = 2.1, particle diameter d_P = 243 μm, Re ≈ 30000, centreline velocity u_c = 17.4 m/s.

ity in this case.

The gas velocity profile is also predicted quite well when considering collisions. In the pipe centre, however, a local minimum in the measured gas velocity is found which is not covered by the simulation. The most probable reason for this lies in the non-consideration of particle rotation in the calculations. The rotating motion of particles induced by particle-wall collisions in an upward gas flow (the gas being the faster phase) induces an asymmetrical local pressure field around the particles. This disturbance leads to the transverse Magnus force driving the particles towards the channel centre. Hence the particle concentration in the centre increases which decelerates the gas due to the increased drag force and lower particle velocity. Thus, between the pipe centre and wall there is a region of lower particle concentration, lower drag and thus, higher gas velocity.

For case IIc the velocity profiles are presented in figure 9. Particles of 243 μm in diameter were used. The particle velocity is underestimated in the centre and over most part of the cross section by circa 10% and slightly overpredicted close to the wall when applying the collision model. The calculated profile is too flat, the predicted homogenisation too strong. When simulated without collisions the particle velocity in the pipe centre matches well, but near the wall the decay becomes too steep.

The gas velocity is reproduced very well with only minor deviance. The maximum velocity is slightly lower when using the collision model and coincides with the experimental value. Close to the wall the measured data are somewhat below the calculated results. The influence of the Magnus force is less pronounced for smaller particles since their wall-collision induced rotational motion is damped faster by the viscous fluid, since their interia is lower. Thus particle rotation is expected to cease in the vicinity of the wall.

The possible sources of discrepancy between experimental and calculated results will be summarised in the following. Concerning the simulation, besides the non-consideration of particle rotation and the effect of Magnus force, it has to be mentioned that the gas turbulence is not altered by the presence of particles in ANSYS CFX. In reality the turbulence is changed, especially at such high particle loadings. Particles can both augment and dampen gas turbulence with consequences on the mean velocities of gas and particles.

A number of points ought to be made regarding the acquisition of experimental data. Firstly, the LDA technique was not technically mature at the time of the experiment (1984). Furthermore the mass loading of the flow was quite high which in combination with the low particle density led to a high particle volume concentration impeding the laser beam.

A two-phase flow workshop, Börner *et al.* (1985), concluded that this experiment does not provide sufficient information on the flow; gas and particle velocities were measured under different test conditions. The measurements were only conducted in one plane which was not situated far enough downstream from the obstacles for the flow to be fully developed (at least for the large 3 mm particles which show a deviation of 15% from stationary state). For this reason, our calculations were carried out for a 10 m pipe instead of a 5.11 m one. Differences in the profiles for 5 and 10 m were indeed almost negligible but this could be due to non-consideration of the elbow and forward-facing step at the bottom of the arrangement. Whether this step could secure a full redispersion of the particles after the elbow was not stated or verified by Tsuji *et al.*

An antistatic coating of the smaller particles was said to reduce electrostatic charges during continuous operation. Tsuji *et al.* did not report whether this measure was successful, for instance whether or not electrostatic adhesion to the wall occured. The mass loading of the flow could have been adversely affected.

Barlow & Morrison (1990) doubt the adequateness of the evaluation technique used by Tsuji *et al.* for highly loaded gas-solid flows. The problem is caused by the non-uniform laser beam intensity in the measuring volume. A distinction between signals of tracer particles for the gas and others of the larger particles on the basis of the signal amplitude alone as conducted by Tsuji's group is not sufficient. The experimental data could thus be distorted.

Moreover, Kartushinsky & Michaelides (2004) point out that the accuracy is reduced near the wall. Nonetheless it has to be stated here that despite the aforementioned uncertainties this experiment is a standard validation case referenced in numerous publications in the literature.

Case III

The third validation case for the implemented collision model is a strongly swirling two-phase pipe flow incorporating a forward facing step. The configuration is shown in figure 10 including the five measurement traverses marked by thick lines. The diameter of the larger pipe is 120 mm, its length 812 mm, and the smaller pipe has a diameter of 96 mm.

The experiment was conducted by Zhou *et al.* (2000) acquiring the data by Phase Doppler Anemometry (PDA) which is capable of providing detailed information on par-

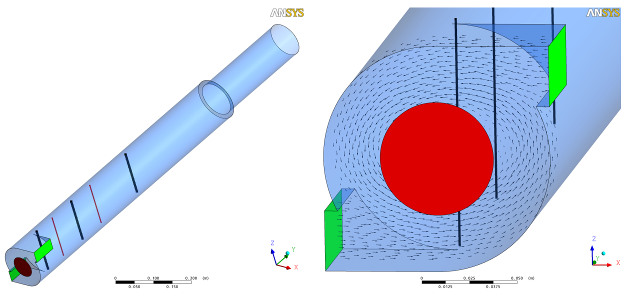

(a) Simulated geometry (b) Inlet region

Figure 10: Geometry of validation case III investigated by Zhou *et al.* (2000).

ticle velocity, diameter and concentration. These measurements were collected along the pipe diameter at five axial positions where those at 82, 227 and 455 mm downstream of the inlet are used for comparison in the diagrams below, marked by thick black lines in figure 10.

All the measurement planes are situated in the forward half of the main pipe of larger diameter, the influence of the forward facing step further downstream is thus assumed to be weak.

The two-phase flow comprises air and glass particles. The air is fed through both the two lateral inlets, marked green in figure 10 and 68 mm $\times$ 32 mm in size, at 10 m/s and through the central axial inlet, marked red and 60 mm in diameter, at 5 m/s. The particles are injected through the axial inlet spreading slowly at first and then being transported to the pipe walls by the centrifugal forces induced by the swirling gas flow. Hence helical particle strands form on the walls. The asymmetry of the flow, the central particle feed as well as the spiral particle streaks are displayed by means of the particle number density in figure 11(a) in the medial plane 288 mm from the inlet. The nominal particle mass loading at the axial inlet at 0.01 is quite low but the induced swirl causes considerably higher values near the wall requiring the application of the inter-particle collision model.

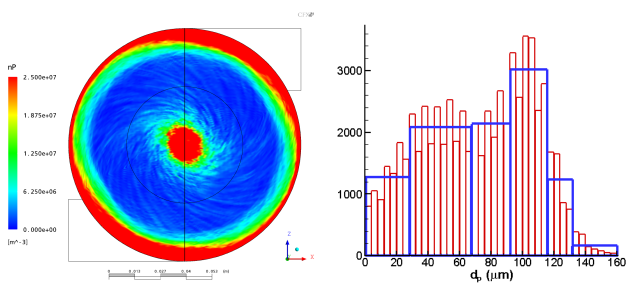

(a) Particle number density (b) Diameter distribution

Figure 11: Particle number density in the cross section y = 288 mm (a), truncated scale. Particle diameter distribution (b) from the measurement (red) and simplified distribution used in the simulation (blue).

Zhou *et al.* (2000) investigated a total of three swirl numbers S: 1.0, 1.5 and 2.1 where only the second case $S = 1.5$ was selected for validation. For each measurement plane, 25 to 35 data points across the pipe diameter were reported except on the plane furthest downstream. There the particle loading on the axis was too low to avoid noticable statistical fluctuations due to the centrifugal effect of swirl. The gas velocity as well as the particle velocity for two diameter classes were measured, collecting 2000 to 5000 measurements per data point.

The experimental particle diameter distribution consists of 40 classes and was simplified to a six-class distribution for the simulation as indicated in figure 11(b). The mean diameter was 76.3 μm. To determine the gas velocity, particles smaller than 10 μm were selected as tracer particles.

At the forward facing step, particles coalesce and move over the step undergoing particle-wall or inter-particle collisions. In the simulation, the step was slightly chamfered to enhance the inward movement of the particles. Interestingly calculations without activated particle collision model refused to converge in stationary simulations. The particles in this case were not able to notice each other, hence trying to move beyond the step by only particle-wall collisions. Despite the chamfer, a large number of particles were caught at the step leading to non-compliance of the mass balance. Not until applying the collision model could convergence of the calculations be observed. The inter-particle collisions led to a immense number of interactions near the step where particles accumulate, homogenising the flow and lifting particles inward over the step. Hence for this test case the collision model is indispensible. Nonetheless a minor error of 1.5% in the mass balance remained.

Owing to the strong anisotropy of the gas turbulence in a swirling flow, a Reynolds stress model was applied in the simulation of this case. This is in contrast to the two-equation models assuming isotropy employed in the first two validation cases. According to the higher number and complexity of the coupled partial differential equations, one has to accept the lower robustness and slower convergence of the numerical calculations. Preliminary tests highlighted excessive damping of the swirl when applying a two-equation model.

The gravitational force was incorporated after communication with the original author Zhou since the orientation of this force in the experiment was not clear from his publication. Gravitation acted against the flow direction, thus being without influence on the flow profiles in circumferential direction. Moreover this slows down axial velocities alleviating the accumulation of particles in front of the step. Besides gravitational and drag forces as well as dispersion, collisions between particles and with walls were considered with a coefficient of restitution of $e = 0.96$. This corresponds to glass particles on acrylic glass of which the pipe was manufactured. Losses arising through parallel wall collisions were neglected.

The high concentration of particles near the wall due to the centrifugal force leads in reality to a large number of particle wall collisions which create particle rotation. This was as mentioned above not considered in these calculations. Hence forces due to particle rotation or influencing rotation are not accounted for, degrading the prediction performance for this case. Also potential deposits of particles at the wall or in front of the step cannot be taken into account at this stage.

The computational grid comprised more than 1.5 million elements with 60000 particle trajectories calculated per iteration.

For comparison, mean and fluctuation velocity profiles in the axial and tangential direction are presented. This is done for three cross sections at 82, 227 and 455 mm from the inlet, the first, third and fifth measurement plane in case 2 of Zhou *et al.*, completed by the particle number density profiles across the pipe diameter.

The swirl number S is given by Zhou *et al.* according to

$$S = \frac{\int_0^{2\pi} \int_0^{R_{\text{in}}} \rho_{\text{gas}}\, v_{\text{gas, tan}}\, v_{\text{gas, ax}}\, r^2\, dr\, d\varphi}{R_{\text{pipe}} \int_0^{2\pi} \int_0^{R_{\text{in}}} \rho_{\text{gas}}\, v_{\text{gas, ax}}^2\, r\, dr\, d\varphi} \qquad (6)$$

and is stated to equal 1.5 in the experiment, where R_{in} is the radius of the axial inlet and R_{pipe} is the radius of the larger pipe. In their paper, Zhou *et al.* do not mention in which cross section the number was determined. In the simulation the swirl number varied with axial position between 1.2 and 1.4 in the region of the tangential inlets, rising to values above 3.1 near the second measurement plane and declining thereafter to 1.7 near the forward facing step indicating dissipative effects. A decreasing swirl number involves a rise in the axial momentum flux leading to increasing axial and diminishing tangential velocities along the pipe.

Depending on the reference radius of the axial momentum flux completely different values of S are obtained, so a comparison to the value indicated by Zhou *et al.* is difficult. For the upper bound of the integral in the numerator of equation (6), R_{pipe} instead of R_{in} was used since the swirling motion takes place in the whole pipe while the axial momentum flux being determined with R_{in} is at first only generated by the axial inlet. Interpretation of the unchanged equation (6) yielded swirl numbers that were too small.

Figure 12 shows the axial mean velocities in the three planes of comparison. In the first plane the particle mean axial velocity is predicted reasonably well except for the maxima at $r = \pm 50$ mm which turn out to be too high. However the gas velocity in the simulation is too high near the pipe centre. Close to the walls a backflow can be observed which was not detected in the experiment. A reason for this could be that the PDA-technique is not capable of yielding an adequate resolution near the wall. In a qualitative sense, according to the profile a congruence between measured and calculated values can also be diagnosed for the gas phase. The gas velocity is above the particle velocity since the gas flow of the two tangential inlets is added to the axial inlet air flow, to which the particles at first flow isokinetically. According to their inertia, it takes a longer time for the particles to adopt their velocity, as can been found from the lower subfigures.

In the second plane at $y = 227$ mm, a homogenisation of the profiles can be observed as the influence of the axial inlet subsides and a Rankine vortex is established. The axial particle mean velocity profile is well reproduced qualitatively but it is overvalued and does not decline enough towards the walls. The gas velocity also is too high, both in the centre and near the walls. Only at half the pipe radius its order of magnitude agrees with the experimental data. The W-shaped profile in the simulation is only observed at a higher swirl number of $S = 2.1$ in the measurements. For the case of $S = 1.5$, the measured profile is more uniform and U-shaped.

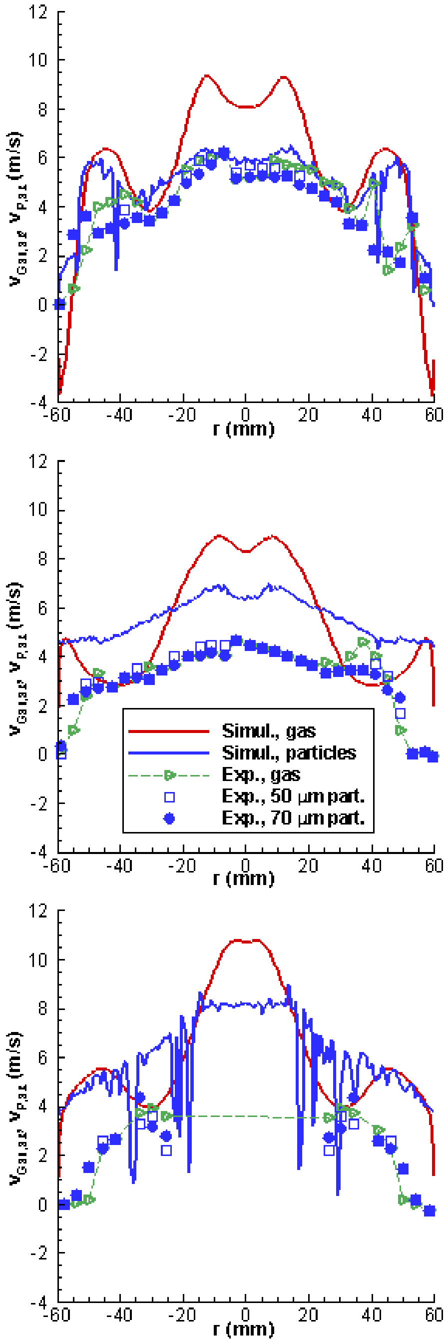

Figure 12: Axial mean velocities of gas and particles (50 and 70 μm in diameter, resp.) as a function of axial position (planes $y = 82, 227, 455$ mm from top to bottom).

This trend continues in the last measurement plane. Also here, the values of the axial mean velocities of air and particles are overpredicted in the calculations. Interestingly in some regions the particles are faster than the gas, however it is where their concentration is low. This is presumably due to the particle inertia as the gas velocity homogenises and decreases more quickly. It can be seen from the fluctuations in the profiles of the last plane that the statistics are insufficient as most particles are already centrifuged outwards and located near the wall. In the measurements less slip between air and particles is found keeping in mind, however, that rather large tracer particles were used, also being subject

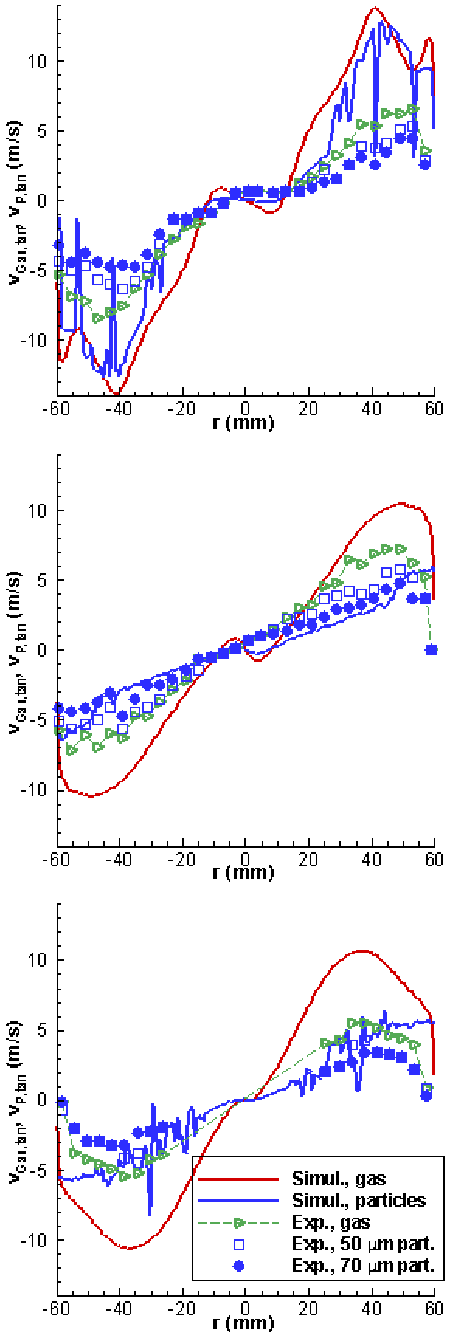

Figure 13: Tangential mean velocities of gas and particles (50 and 70 μm in diameter, resp.) as a function of axial position (planes $y = 82$, 227, 455 mm from top to bottom).

to centrifugal forces.

The mean tangential velocity is depicted in figure 13. The profiles for the first plane show a good agreement for the particle velocity over most of the diameter. Only close to the wall there are larger fluctuations than in the experiment, in part due to statistical inaccuracy by reason of a low particle number. The too high near-wall particle velocities indicate the improper neglect of wall friction in the simulation – parallel to the wall losses are not accounted for. Due to their inertia the particles have a lower circumferential velocity than the air both in the calculations and in the experiment, yielding slip. Qualitatively the gas velocity profile is predicted correctly in all three planes of comparison, but similar to its axial counterpart, its absolute value is too high in the simulation.

In the experiment as well as in the calculations, the decrease of tangential velocity along the pipe axis is apparent being a consequence of the declining swirl as a result of dissipation. In the second plane, the maximum of the tangential particle velocity is overvalued and located radially too far off-axis; in the last plane, its radial position is closer to the measured data. Clearly a Rankine vortex is observed, only the no-slip condition at the wall decelerates the flow. The oscillating profile in the simulation in the last plane is again an outcome of the poor statistics away from the wall due to the lack of particles.

While the mean velocities tend to be too high in the calculations, it can be observed from figure 14 that the standard deviation of particle velocity fluctuations (RMS-values) in the axial direction is underestimated. For the particles the values in the first plane are almost half an order of magnitude below those of the experimental data, without any qualitative agreement.

The fluctuation velocity of the gas phase in the axial direction is in most parts considerably higher than that of the particles. Nevertheless the high experimental values are not reproduced and, qualitatively, the profiles do not agree. In the second plane of comparison the results are better but the peak in the experimental fluctuating velocity at $r = +45$ mm is not reproduced. Here the particle velocity fluctuations are predicted to be too low; in the plane furthest downstream there is better accordance between simulation results and experiment. The calculated profile of axial particle fluctuations is, however, more homogeneous than the measured one. The axial fluctuations tend to be somewhat augmented near the wall compared to the pipe centre.

The tangential component of the velocity fluctuations is depicted in figure 15. In the plane at $y = 82$ mm the profiles of tangential particle velocity fluctuations agree at least qualitatively and the local maxima are predicted at coinciding radii. In addition the predicted absolute value is too low. The fluctuations of the circumferential air velocity are greater than those of the particles in the experiment. The profile, however, resembles the measured values only vaguely.

Further downstream the particle velocity fluctuations exceed those of the gas-phase in the outer third of the radius. This phenomenon occurs in the measurements and is reproduced by the calculations as well. In the pipe centre away from the inlets, on the other hand, there are few particles left so their fluctuations in the calculation are very weak.

In the second and the last plane the tangential gas-phase velocity fluctuations are reproduced fairly well even though the local maxima are not met exactly. Generally it can be recognised that the fluctuations are anisotropic which justifies the application of a Reynolds-stress turbulence model. The axial fluctuations of the particle velocity is in most regions higher than the tangential compound; for the gas-phase there is no consistent trend in this regard.

Altogether the measurements show that smaller and thus less inertial particles experience larger velocity fluctuations, both in the axial and tangential direction. The same is true for

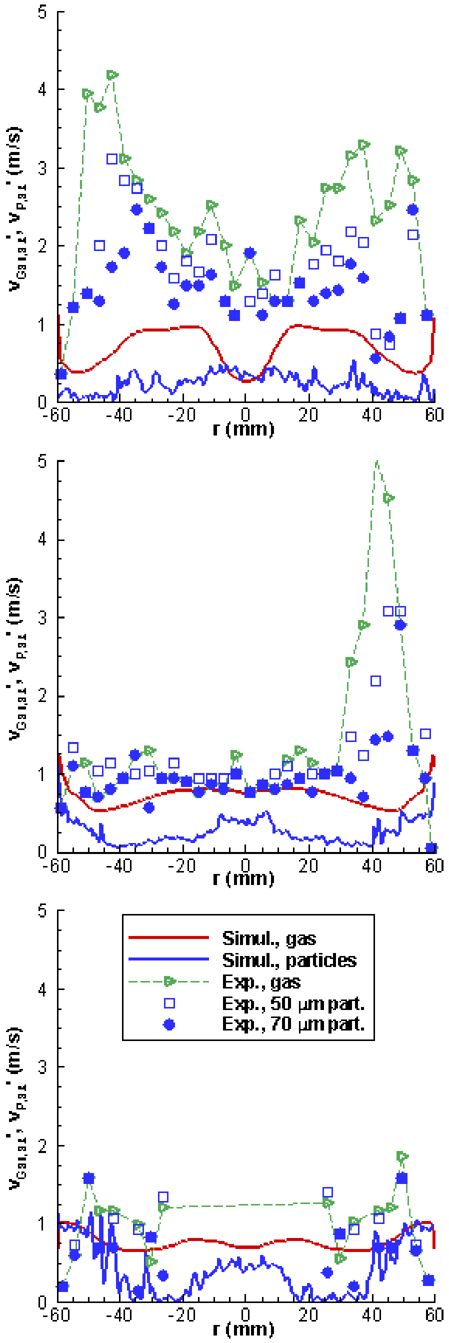

Figure 14: Axial velocity fluctuations (RMS-values) of gas and particles (50 and 70 μm in diameter, resp.) as a function of axial position (planes y = 82, 227, 455 mm from top to bottom).

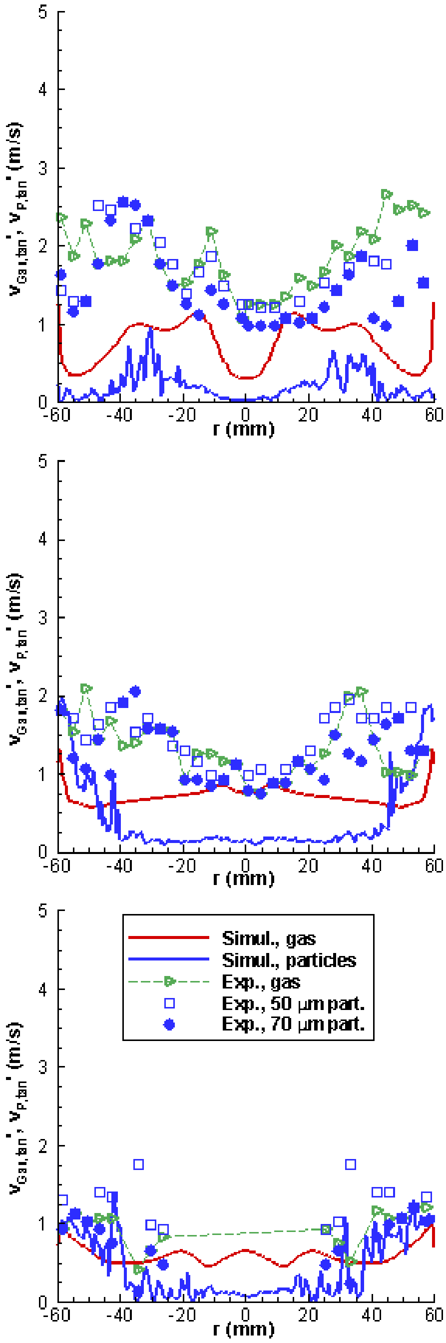

Figure 15: Tangential velocity fluctuations (RMS-values) of gas and particles (50 and 70 μm in diameter, resp.) as a function of axial position (planes y = 82, 227, 455 mm from top to bottom).

the mean velocities of the particles. For the case 3 ($S = 1.0$), Zhou *et al.* investigated that the slip velocity between gas and particles in the radial direction is very low. In summary the tangential velocity components are predicted reasonably well for gas and particles whereas the axial velocities deviate considerably from the measured data. For the mean velocities the simulation yields values too high and for the fluctuating parts values too low.

Finally the particle number density n_P displayed in figure 16 is selected for comparison. Most likely there is an error in the presentation of the data in figure 18 on page 84 in Zhou *et al.* (2000) where the shown experimental data seem to be too high by a factor of 10. The data presented in this work display the corrected values and show good agreement in the first two planes. A further suggestion of the erroneous original presentation is that the experimentors also reach values for their case 1 ($S = 2.1$) with a similar geometry and boundary conditions that are an order of magnitude lower than the values indicated for case 2 ($S = 1.5$); such a difference could not be explained.

Comparing the results of the calculation with the corrected experimental data, a high particle concentration can be ob-

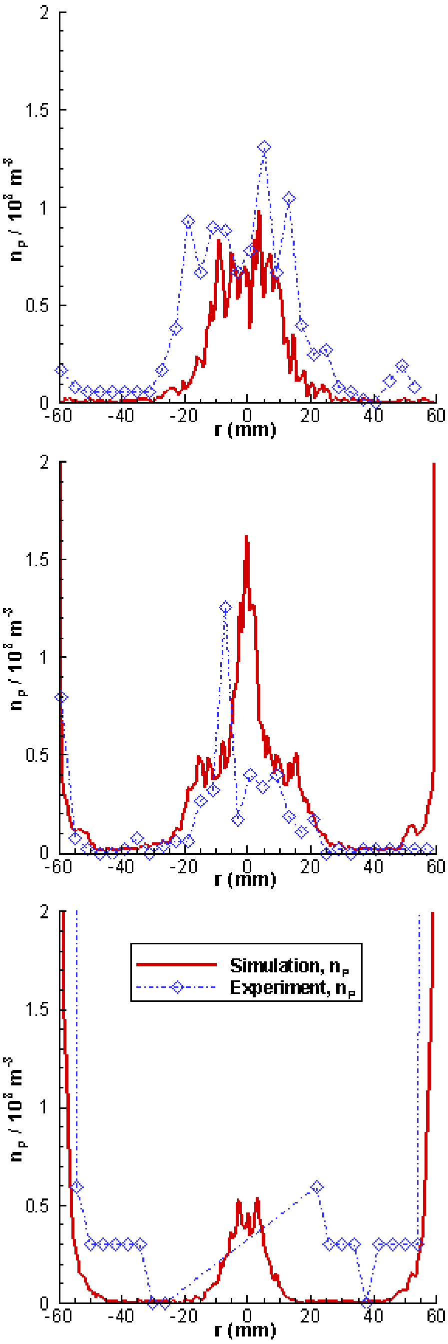

Figure 16: Particle number density as a function of axial position (planes $y = 82, 227, 455$ mm from top to bottom).

served in the first plane near the pipe axis. This can be explained because the particles are fed solely through the axial inlet. The simulation reproduces the profile quantitatively. The main peak is slightly wider in the experiment but is also reproduced well.

In the second plane at $y = 227$ mm the influence of the centrifugal forces becomes apparent by a sudden increase of the number density near the wall. The height of this jump is also quantitatively well reproduced at the side of negative radius; on the opposite side the measured data do not show such a peak. This might be due to a different course of the particle strands on the wall or to the relatively low measurement resolution near the wall, i.e. the accumulation of particles may be located closer to the wall as is predicted in the simulation. The maximum of the number density equals $5.3 \cdot 10^8$ directly at the wall.

Since a fraction of the particles is already centrifuged outwards in this plane the local maximum in the pipe centre is narrower than in the first plane. The peak shown in the experiment is also calculated correctly, albeit symmetrical and not shifted to the left as in the measurements.

The last subfigure shows the concentration profile in the last measurement plane in which almost all particles are situated close to the wall. The peaks are out of the shown scale: In the simulation values up to $7.9 \cdot 10^8$ are obtained while even $2.6 \cdot 10^9$ is reached in the experiment after correction. In the pipe centre a small local maximum remains. The reading accuracy of the measured values is worsened by a factor of 10 due to the changed presentation scale of the original data. Hence values shown here to be $0.3 \cdot 10^8$ could be nearly zero in reality. The higher point at ca. $r = 20$ mm indicates that in the experiment, particles still flow in the pipe centre at this axial position.

Some of the deviation between calculation and experiment could be explained, if the mass loading stated in Zhou *et al.* (2000) did not refer to the overall air mass flow, but only to the central gas inlet. This would give rise to an overall more dilute flow and a less distinct dampening effect of the particles on the air velocity fluctuations. On the other hand, the axial gas velocity would thus increase even more.

Conclusions

This article presents the stochastic particle-particle collision model implemented into the commercial CFD-package ANSYS CFX for simulating dense gas-solid flows in the Lagrangian frame of reference. The merits of this model leading to so-called four-way coupling is a considerably improved description of dense gas-solid two-phase flows.

In the first part, the algorithm of the collision model developed by Oesterlé & Petitjean and improved by Sommerfeld is described. The second part shows the effects of this model and its potential for an improved simulation of highly-loaded gas-solid flows by means of comparison with measurement data from three experiments reported in the literature.

The first test case (Fohanno & Oesterlé) consists of a vertical convergent channel providing a good basis for model testing since it enforces collisions by virtue of its design. As coarse particles were used during the measurements, the effect of turbulence is rather low. The second comparison was carried out with experimental data of Tsuji *et al.* on a vertical two-phase pipe flow which served as validation basis for several studies in the literature. The last case originates from Zhou *et al.* who investigated a strongly swirling gas-particle pipe flow. Due to the anisotropy of the fluctuating quantities a Reynolds stress turbulence model was applied in the simulation.

It is shown that the newly implemented particle-particle collision model in ANSYS CFX leads to a considerably improved description of highly-loaded gas-solid flows. Calculation of particle rotation was neglected for the time being.

Comparison with numerical results of Pachler who applied the same model incorporating particle rotation in a university CFD-code displayed a slight improvement of the predictions when accounting for rotation.

In case of flows dominated by particle-wall collisions, provision for rotation is advisable. This kind of collision involving friction induces particle rotating motion that also evokes transverse forces such as the Magnus effect. This is the case for swirling pipe flows and horizontally confined flows due to the centrifugal and gravitational forces, respectively. Strong fluid velocity gradients as those occurring near the inlets of case III also lead to an impact on the particle motion according to a transverse lift force (Saffman force). This force is not included in ANSYS CFX at present. Hence the results leave room for impovement by additional incorporation of particle rotation, frictional particle-wall collisions and the Saffman force.

Nevertheless the implemented model yields satisfactory results in the framework of engineering accuracy with only minor additional computational effort. As a rule the CPU-time of the Lagrangian solver is augmented less than twofold, certainly depending on the mass loading and flow geometry. The model represents a major advance in the simulation of dense gas-particle flows in commercial CFD-solvers and will be fully supported and accessible in the GUI from the forthcoming version (CFX 12) on.

Acknowledgements

The authors greatly appreciate the financial support of this project by Bayern-Chemie Protac GmbH.

References

Barlow, R.S. & Morrison, C.Q. Two-phase velocity measurements in dense particle-laden jets. Experiments in Fluids, Volume 9, 93 – 104 (1990)

Börner, Th., Durst, F. and Milojevic, D. (editors). Second workshop on two-phase flow predictions, Lehrstuhl für Strömungsmechanik, University of Erlangen-Nuremburg, Erlangen, May 22–24, (1985)

Fohanno, S. & Oesterlé, B. Analysis of the effect of collisions on the gravitational motion of large particles in a vertical duct. Int. J. Multiphase Flow, Volume 26, 267 – 292 (2000)

Frank, Th. Parallele Algorithmen für die numerische Simulation dreidimensionaler, disperser Mehrphasenströmungen und deren Anwendung in der Verfahrenstechnik. Shaker Verlag, Aachen, 2002. Technical University Chemnitz, Habilitation thesis (2002)

Kartushinsky, A. & Michaelides, E.E. An analytical approach for the closure equations of gas-solid flows with inter-particle collisions. Int. J. Multiphase Flow, Volume 30, 159 – 180 (2004)

Lavieville, J., Deutsch, E. & Simonin, O. Large eddy simulation of interactions between colliding particles and a homogeneous isotropic turbulence field. ASME FED Volume 228, 359–369 (1995)

Oesterlé, B. & Petitjean, A. Simulation of particle-to-particle interactions in gas-solid flows. Int. J. Multiphase Flow, Volume 19(1), 199 – 211 (1993)

Pachler, K. Parallele Berechnung 3-dimensionaler, instationärer Gas-Partikel-Strömungen unter Berücksichtigung von Kollisionen und Aggregatzustandsänderungen. Dissertation, Technical University Chemnitz. Shaker Verlag, Aachen (2004)

Sommerfeld, M. The importance of inter-particle collisions in horizontal gas-solid channel flows. ASME FED Volume 228, 335–345 (1995)

Sommerfeld, M. Validation of a stochastic Lagrangian modelling approach for inter-particle collisions in homogeneous isotropic turbulence. Int. J. Multiphase Flow, Volume 27, 1829 – 1858 (2001)

Tsuji, Y. & Morikawa, Y. LDV measurements of an air-solid two-phase flow in a horizontal pipe. J. Fluid Dynamics, Volume 120, 385 – 409 (1982)

Tsuji, Y., Morikawa, Y. & Shiomi, H. LDV measurements of an air-solid two-phase flow in a vertical pipe. J. Fluid Dynamics, Volume 139, 417 – 434 (1984)

Tsuji, Y., Morikawa, Y., Tanaka, T., Nakatsukasa, N. and Nakatani, M. Numerical simulation of gas-solid two-phase flow in a two-dimensional horizontal channel. Int. J. Multiphase Flow, Volume 13, No. 5, 671 – 684 (1987)

Zhou, L.X., Li, Y., Chen, T. & Xu, Y. Studies on the effect of swirl numbers on strongly swirling turbulent gas-particle flows using a phase-Doppler particle anemometer. Powder Technology, Volume 112, 79 – 86 (2000)